Accurate single-shot quantitative phase imaging of biological specimens with telecentric digital holographic microscopy

Ana Doblas,[a,*] Emilio Sánchez-Ortiga,[a] Manuel Martínez-Corral,[a] Genaro Saavedra,[a] and Jorge Garcia-Sucerquia[a,b]
[a]University of Valencia, 3D Imaging and Display Laboratory, Department of Optics, E-46100 Burjassot, Spain
[b]Universidad Nacional de Colombia Sede Medellin, School of Physics, A.A. 3840, Medellin 050034, Colombia

Abstract. The advantages of using a telecentric imaging system in digital holographic microscopy (DHM) to study biological specimens are highlighted. To this end, the performances of nontelecentric DHM and telecentric DHM are evaluated from the quantitative phase imaging (QPI) point of view. The evaluated stability of the microscope allows single-shot QPI in DHM by using telecentric imaging systems. Quantitative phase maps of a section of the head of the drosophila melanogaster fly and of red blood cells are obtained via single-shot DHM with no numerical postprocessing. With these maps we show that the use of telecentric DHM provides larger field of view for a given magnification and permits more accurate QPI measurements with less number of computational operations. [DOI: 10.1117/1.JBO.19.4.046022]

Keywords: digital holographic microscopy; quantitative phase imaging; aberration compensation.

Paper 130606R received Aug. 19, 2013; revised manuscript received Dec. 9, 2013; accepted for publication Mar. 31, 2014; published online Apr. 29, 2014.

1 Introduction

Label-free quantitative phase imaging (QPI) of transparent microscopic specimens is the distinctive hallmark of digital holographic microscopy (DHM). This unique feature has been determinant to find applications of DHM in living cell screening,[1–4] particle tracking,[5–11] and MEMS evaluation,[12–14] among many others.[15–24] The ability of performing QPI has been extended to other microscopy methods like spatial light interference microscopy or spatial light interference tomography;[25,26] hence similar applications have been reported by the use of these imaging approaches. In DHM, the fringe pattern recorded after the interference between a reference wave and the image of the wave diffracted by the microscopic sample allows the retrieval of the phase changes introduced by the sample. These phase changes encode the information about the refractive index and thickness of the specimen; therefore their accurate measurement is determinant in the different applications where DHM can be utilized. Cell volume,[15–17] osmotic membrane water permeability coefficient,[18] and the integral intracellular refractive index[17,19] are some of the quantitative biological parameters that can be evaluated with DHM via the phase retrieving of the sample. DHM combined with digital video microscopy is also an effective tool to fully localize in three-dimensions living cells in controlled or natural environments[9–11] as a way to derive insight about the cell behavior. Its unique feature of label-free imaging of cells has turned DHM into a suitable tool for cell sorting and counting.[20,21] All the above examples of application of DHM relied on the QPI; hence, the accuracy of the phase-map measurements could be determinant on a disease diagnostic and/or specimen identification.

DHM is a hybrid imaging method in which the final image is obtained after an optical recording procedure and a subsequent computational reconstruction process. In DHM, the QPI is obtained from raw phase maps, which are computed from the reconstructed complex object wave. Therefore, the recording and reconstruction processes of such complex amplitude determine the accuracy of the QPI. Owing to DHM being a holographic method,[27–30] the computational reconstruction of the object wave follows well-established and exact methods,[27–30] so that one can state that DHM can retrieve the recorded object wave with almost no distortion. In these terms, the recording of the object wave controls the accuracy of the QPI-DHM, as it has been recently analyzed in Ref. 31. In that work, the authors have pointed out that in regular DHM microscopes operating in nontelecentric mode, the recorded object wave carries the phase change introduced by specimen superimposed with the residual quadratic phase factor, whose curvature depends on the distance that exists between the aperture stop of the microscope objective (MO) and the tube lens (TL) plane.[31,32] To obtain, after a computational process, an accurate reconstruction of the phase changes introduced by the specimen, the effects of that residual quadratic phase distortion must be removed. Different numerical methods have been proposed to remove *a posteriori* these effects.[33–36] However, even after applying such methods, it is common to find a remaining phase factor that still perturbs the QPI measurement. In addition to that remaining phase factor, when the recording setup operates in the nontelecentric mode,[31] the DHM is shift-variant.[31,37] This means that the accuracy of the QPI measurements strongly depends on the position of the sample in the field of view (FOV).

The effects of the nontelecentric recording systems can also be suppressed *a priori* by introducing twin-imaging systems for the reference and objects waves,[38] but it requires the very precise alignment of two identical complete imaging systems and

*Address all correspondence to: Ana Doblas, E-mail: a.isabel.doblas@uv.es

doubling the cost of the microscope. A second approach to remove the residual quadratic phase distortion can be achieved by *a posteriori* point-wise subtraction of the measured phase with no sample placed from the measurement with the sample in place.[39] The main drawback of this latter method is that it requires two shots, which is not always possible like *in vivo* measurements. A simple and effective way of avoiding theses detrimental effects in a single shot way is by setting up the recording system in telecentric mode, so that the quadratic phase factor is not produced.

Other methods to provide QPI take advantage of the telecentric design of the modern commercial microscopes. Diffraction phase microscopy and Fourier phase microscopy, both using white light, have been presented recently operating on the framework of the commercial microscopes in telecentric configuration.[40,41] DHM has also been proposed operating over commercial microscope; however, for unknown reasons, the resulting DHM operates on nontelecentric configuration;[36] hence, intense *a posteriori* numerical processing is needed to alleviate the perturbation introduced by the imaging system. Even though the telecentric imaging systems in DHM were introduced several years ago[32] and some of the special features that are derived from its use have been reported,[31] they are not widely used in DHM, and therefore, the advantages that their utilization provides in QPI-DHM of biological specimens still have to be presented and highlighted.

The aim of this work is to demonstrate and emphasize that the QPI-DHM working in the telecentric mode provides much more accurate phase maps of biologic samples than the ones working in the conventional nontelecentric regime. By evaluating the stability of the microscope, we show that if the imaging system operates in telecentric mode, single-shot QPI of biological specimens is possible with great accuracy and at minimum postprocessing. On the contrary, we will show that when a DHM operates in nontelecentric regime the perturbations introduced by the imaging system lead to distorted QPIs, even if intense postprocessing of the raw phase map is made. QPI-DHM working in the telecentric mode can provide the biomedical community with high-resolution, nondistorted phase images, which can be very useful for the diagnosis or screening of different diseases; biologist can also be provided with trustable tool for specimen identification. To this end, in this work, the performances of telecentric DHM and nontelecentric DHM are compared in terms of accuracy of the QPI measurements carried out on biological specimens with very different sizes. In our first experiment, a section of the head of a drosophila melanogaster fly, 800 μm in width and 8 μm in thickness, is imaged with low magnification. In the second experiment, human red blood cells (RBC) ~10 μm in diameter and between 0.8 and 2.5 μm in thickness are imaged with high magnification QPI-DHM. The obtained experimental results demonstrate the superiority of the telecentric mode for the study of biological samples.

2 QPI-DHM for Biological Specimens Millimeter-Sized

Let us start this section by describing the image formation performed in QPI-DHM.[31] The setup is based on a Mach-Zehnder interferometer. An He-Ne laser of wavelength $\lambda = 633$ nm is split to produce the reference (R) and object waves (O). A CCD camera with 1024×1024 square pixels of 6.9 μm side records the holograms formed by the interference between the wavefield scattered by the object and a titled reference plane wave. In a second beam splitter, the angle between the reference and object waves is controlled to guarantee that the DHM operates in off-axis geometry while the sampling requirements are fulfilled. In the object arm, the wavefield scattered by the object is enlarged over the surface of the CCD by using an adjustable imaging system composed of a microscope objective (MO) and a tube lens (TL). A complete schematic representation of the experimental setup is shown in Fig. 1.

As it has been mentioned above, the computational processing of the digital holograms in DHM has evolved up to such level of quality that one could state that if the sampling conditions are fulfilled,[42] the optical object wavefield recorded by the DHM could be retrieved with no perturbation. This advance allows the user of the DHM to focus on studying the complex object wavefield recorded by the DHM. By using regular imaging ABCD transformations,[43] the object wave O recorded on the CCD camera is given by

$$O(x,y) = \frac{-1}{M}\exp\left[i\frac{2\pi}{\lambda}(f_{\mathrm{TL}} + f_{\mathrm{MO}} + d)\right] \times \exp\left[i\frac{\pi(f_{\mathrm{TL}} - d)}{\lambda f_{\mathrm{TL}}^2}(x^2 + y^2)\right] \times \left[O'\left(\frac{x}{M}, \frac{y}{M}\right) \otimes_2 \tilde{P}\left(\frac{x}{\lambda f_{\mathrm{TL}}}, \frac{y}{\lambda f_{\mathrm{TL}}}\right)\right]. \quad (1)$$

In this equation, O' and $\tilde{P}$ represent, respectively, the complex amplitude scattered by the object and the Fourier transform of the MO aperture stop. The sign $\otimes_2$ stands for the two-dimensional convolution product, and λ is the illumination wavelength. The magnification of the system, $M = -f_{\mathrm{TL}}/f_{\mathrm{MO}}$, is obtained as the quotient between the focal length of the TL and the one of the MO. Finally, d is the distance between the MO aperture stop and the TL. As DHM operates in nontelecentric mode, the recorded complex object wave represented by Eq. (1) carries the quadratic phase factor $\exp[i\pi(f_{\mathrm{TL}} - d)/\lambda f_{\mathrm{TL}}^2(x^2 + y^2)]$ superimposed with the phase of the sample itself. This phase factor is then numerically eliminated by means

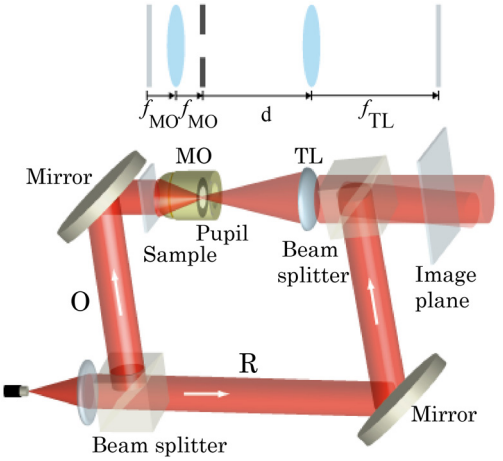

Fig. 1 Illustration of the transmission digital holographic microscopy (DHM) used to evaluate quantitative phase imaging (QPI) measurements. The setup follows an off-axis architecture. The DHM operates in a telecentric or nontelecentric regime depending on the configuration between the microscope objective (MO) and tube-lens (TL).

of *a posteriori* processing of the recovered object phase. Unfortunately, as we show in the paragraphs below, the numerical postprocessing could not always remove fully the effects of that phase factor, leading to perturbed phase maps. However, as the DHM operates in telecentric mode $f_{TL} = d$ and such additional phase factor vanishes, the recovered phase map exclusively represents the phase of the sample O'. In this way no extra *a posteriori* numerical processing is needed to recover the phase on the object under study.

As phase measurements could be strongly dependent on ambient fluctuations, initially we tested the stability of our experimental setup. To provide a controlled environment for the experiments, the complete microscope has been enclosed in a polymethymethacrylate (PMMA) cage and the temperature of the lab has been controlled. To exclude any incidence of ambient perturbations on the results of the experiment, we have tested our setup by recording 20 experimental holograms for each configuration. The 20 evaluated phase maps for each configuration were averaged and its correlation with respect to each individual phase map was evaluated. For telecentric and nontelecentric configurations, the correlation parameters were 0.991 ± 0.008 and 0.996 ± 0.003, respectively. As both correlation figures are close to 1, we can conclude that microscope is fairly isolated from ambient fluctuations; hence, any divergence between the measurements performed with the telecentric and nontelecentric configuration is due to differences on the performance of the imaging system itself. Additionally, the possibility of needing just a single shot for the QPI-DHM analysis would be determined by the imaging system rather than by external variables.

Our first experiment was prepared for performing QPI-DHM of a millimeter-sized specimen. Then we used a section of the head of a drosophila melanogaster fly, 800 μm wide and 8 μm thick. For large samples like this, the QPI-DHM must operate at low magnification. In particular, we used a $10\times/0.45$ MO corrected at infinity and a TL of focal distance $f_{TL} = 200$ mm. The lateral magnification of the microscopes was $M = -10$. To show the differences between the telecentric and the nontelecentric modes, the DHM was adjusted in two different configurations: $f_{TL} \neq d$ (nontelecentric mode) and $f_{TL} = d$ (telecentric mode).

The first step of the experiment was the recording of the holograms, which is shown in Figs. 2(a) and 2(d). Note that the holograms are intensity recordings, and therefore, the effects of the residual phase factor introduced by the nontelecentric imaging system are not directly visible; thus, the holograms look alike. However, if one observes the Fourier transform of the raw holograms, see the insets in the bottom-right region of Figs. 2(a) and 2(d), the presence of the quadratic phase factor in the nontelecentric imaging system introduces an enlarging of the diffracted orders. In the realization of the computational procedure, the holograms are initially spatially filtered to remove the dc term and the twin image.[44] Next, the filtered holograms are computationally propagated via the angular spectrum approach[27,45] to recover the complex object wave. It is worth recalling that for the case of the nontelecentric DHM, the recovered object wave carries the phase introduced by the object merged with the residual quadratic phase inherited from the recording imaging system. The raw phases computed for both modes of operation of the QPI-DHM are shown in Figs. 2(b) and 2(e). For the telecentric DHM, the recovered phase map reproduces the phase introduced by the sample. Details of the internal structure of the section of the head of the drosophila melanogaster fly are visible clearly.

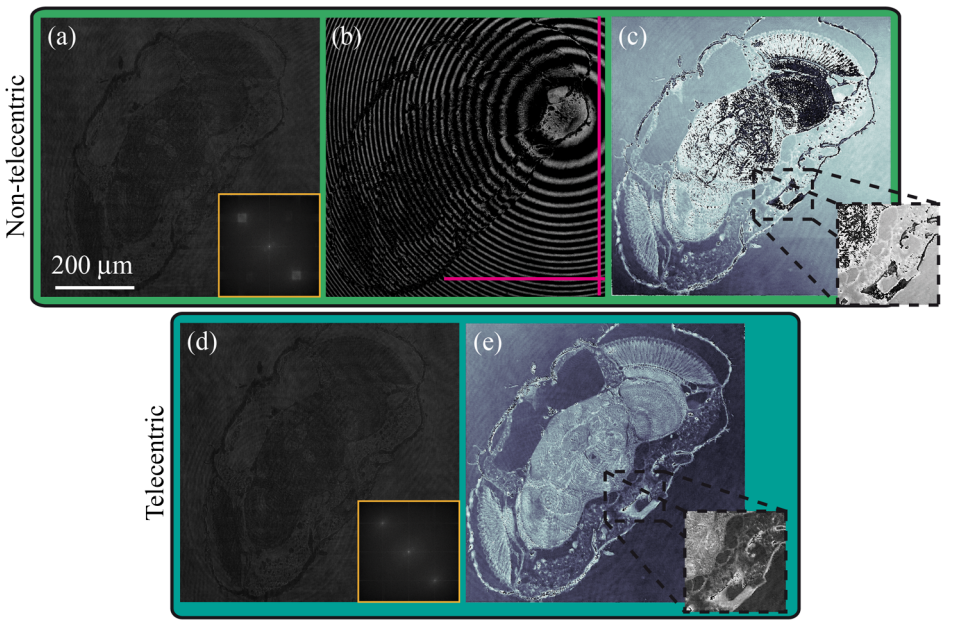

Fig. 2 QPI for a section of the head of a drosophila melanogaster fly at $M = -10$. The first row shows the results for a nontelecentric configuration: (a) Raw hologram. (b) Raw phase image. (c) Numerically corrected phase image calculated from (b). The second row shows the results obtained with the telecentric setup: (d) Raw recorded hologram. (e) Telecentric raw phase image. The light pink lines in (b) correspond to the selected profiles, which are used to extract the data for computing the compensation phase. Also, the Fourier transform of the raw holograms are illustrated in the insets at the bottom-right part of (a) and (d).

The raw phase for the nontelecentric DHM shows a ring-like structure superimposed over the phase map [see Fig. 2(b)]. This effect has been present in all the realizations of DHM since its very origin.[46] As explained above, this drawback, which is caused by the residual quadratic phase factor, can be numerically removed *a posteriori* via a variety of procedures.[33–36] The most utilized methods for removing the residual phase factor are based on polynomial fitting of areas selected from the raw phase where the contribution of object to the phase map is constant.[35,36] This condition imposes the need of areas of the FOV free of sample information, which means a significant reduction of the usable FOV. This situation is illustrated in Fig. 2(b). Owing to the specimen covering almost the complete available FOV, there is just a very limited area left to collect the needed information for the polynomial fitting. The light pink lines plotted in Fig. 2(b) show the selected regions from which the data for computing the numerical phase compensation have been extracted. The computed compensation phase is then subtracted from the raw phase to produce the numerically corrected phase map shown in Fig. 2(c). In this phase map, there are some regions with remaining phase curvature, which introduces perturbation of the phase of the object. The blackish area in this panel is an illustration of the ruining effects of the remaining phase factors. The zoomed-in square areas in Figs. 2(c) and 2(e) show a region in which the results for nontelecentric DHM and telecentric DHM are very different, having the telecentric better resolution and contrast.

For better visualization of the differences between the phase maps produced by the nontelecentric and the telecentric DHM, three-dimensional (3-D) pseudocolor images are shown in Fig. 3. According to the color bar, even for the areas where the phase maps in Figs. 2(c) and 2(e) look alike, there are differences in the measured phases, revealing the *a posteriori* removal of the residual phase rings does not avoid the presence of perturbations in the QPI. This happens in good agreement with the recently proven statement that the QPI measurements provided by the telecentric DHM are more accurate than those obtained from nontelecentric DHM.[31] The highlighted differences for these areas could definitely mislead a specimen identification, which would be supported on the analysis of this particular area of this insect.

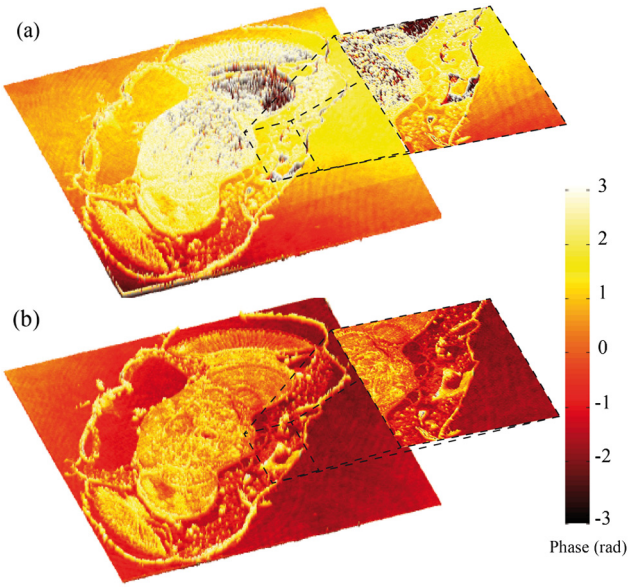

Fig. 3 (a) Three-dimensional (3-D) pseudocolor image of the phase map shown in Fig. 1(c). (b) 3-D pseudocolor image of the phase map shown in Fig. 1(e). In both cases, the image area is 0.707×0.707 mm^2. The insets highlight some of the differences between both phase maps.

At very first glance, one could claim that the difficulties mentioned above can be circumvented if lower magnification is utilized. Low magnification renders a larger FOV and, therefore, more available data for computing the numerical compensation phase. With the aim of checking this alternative, we performed an additional experiment in which the QPI-DHM has been configured to operate at $M = -7.5$. In this, the same $10\times/0.45$ MO is matched with a TL of focal distance $f_{\mathrm{TL}} = 150$ mm. The results of the QPI-DHM operating at this magnification for the same specimen as in Fig. 2 are shown in Fig. 4. The recorded holograms shown in Figs. 4(a) and 4(d) now have larger FOV and, therefore, larger areas free of specimen information. The inset in the holograms representing the Fourier transforms of the holograms show the important enlargement of the diffracted orders for the nontelecentric imaging system in comparison with those for the telecentric setup. The raw phase maps, Figs. 4(b) and 4(e), have larger areas from which the data for phase compensation can be extracted, which leads, after the usual series of *a posteriori* operations,[35,36] to the corrected phase map for the nontelecentric DHM shown in Fig. 4(c). Note that in this case the compensated phase map for nontelecentric DHM looks quite comparable with the raw phase for the telecentric DHM.

Also, in this case, we have represented the phase maps in 3-D pseudocolor, see Fig. 5. In these maps, the square zoomed-in areas show details quite different. The areas that are enclosed by the ellipses reveal a horn-like structure. This feature clearly visible for the telecentric DHM is hardly seen for the nontelecentric-DHM, which could mean a misclassification of the specimen, as it was shown above. These results show that additional extra manipulation of the recovered phases from nontelecentric DHM are needed to obtain a phase map of the object comparable with that obtained from telecentric DHM. For this procedure being effective, the object under study should not cover the complete FOV. Even though when enough FOV is free of sample information, the QPI measurements are perturbed as shown in Figs. 5(a) and 5(b) and analyzed in more detail in the following section.

3 QPI-DHM for Biological Specimens Micrometer-Sized

As stated above, the performance of nontelecentric-DHM and telecentric DHM are more comparable when there is enough FOV free of information from the specimen. In this case, it is possible to collect representative data to calculate the compensating phase and, therefore, the phase map of the object is less distorted by the quadratic phase inherited from the recording system. This scenario is presented, for example, when micrometer-sized objects are imaged with DHM. The performance of QPI-DHM operating in this condition has been evaluated by imaging human RBC. Thus, we prepared a sample by smearing a blood drop on a glass slide. The smeared blood was dried out at room temperature in a dust-free environment. A $50\times/0.55$ MO corrected at infinity and a TL with focal length $f_{\mathrm{TL}} = 200$ mm were utilized for recording the hologram with magnification

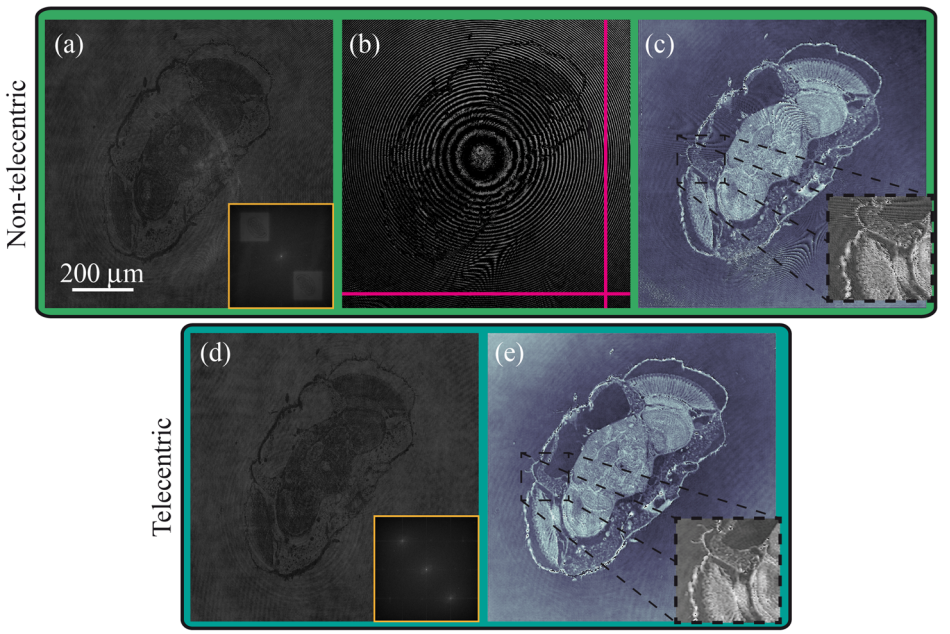

Fig. 4 QPI for a section of the head of a drosophila melanogaster fly at $M = -7.5$. The first row represents the experiment for a nontelecentric configuration: (a) Raw hologram. (b) Raw phase image. (c) Numerically corrected phase image calculated from (b). The second row shows the results obtained with the telecentric setup: (d) Raw hologram. (e) Raw phase image. The light pink lines in (b) correspond to the selected profiles, which are used to extract the data for computing the compensation phase. The Fourier transform of the raw holograms are illustrated in the insets of (a) and (d).

$M = -50$. Again, depending on the value of d, the DHM operate in nontelecentric or in telecentric mode.

The same procedure utilized above to eliminate *a posteriori* the quadratic phase was applied to recover phase maps for the RBCs when operated in the nontelecentric mode. Owing to the RBCs leaving large free areas to gather the needed information for the numerical compensation, the recovered phase maps for the nontelecentric DHM and telecentric DHM look alike, as shown in Figs. 6(a) and 6(c). Despite their similar aspect, in the nontelecentric case, the phase measurements are strongly dependent on the location in the FOV.[31] To see that, the areas inside the pink squares are zoomed in Figs. 6(b) and 6(d). These closer views reveal the following. (1) The reported shift-variant behavior for the nontelecentric DHM is evident. In Fig. 6(b) two individual RBCs are zoomed in and their phase values quantified. As visualized from these zoomed images, there are important differences in the measured phase for the apparently identical RBCs but placed at different regions in the FOV. On considering that the measured phase is related with the thickness of the sample t, the refractive index of the sample n_s, and the surrounding n_m via $\phi = 2\pi/\lambda(n_s - n_m)t$, the distorted phase measurement could mislead illness diagnostic, for instance. (2) The telecentric DHM is a shift-invariant QPI. The same RBCs analyzed for panel (b) are studied in panel (d). As $\lambda = 633$ nm, $n_s = 1.406$,[47] and $n_m = 1$, the measured phase can be converted in specimen's thickness. Inside the experimental errors, which are in the order of ± 0.018 μm, the measured thicknesses for the RBCs placed at different locations in the FOV are the same. (3) Apparent morphological changes are introduced by the nontelecentric DHM. As the zoomed individual RBCs are compared, those reconstructed from the nontelecentric DHM present an internal structure that differs from that seen in the RBCs reconstructed from the telecentric DHM. In summary, even though there is enough free area in the FOV to gather data for computing the compensating phase inherited from the nontelecentric DHM, the numerical *a posteriori* elimination of that phase leaves remains that perturb the QPI. This could mislead this to illness screening, specimen identification,

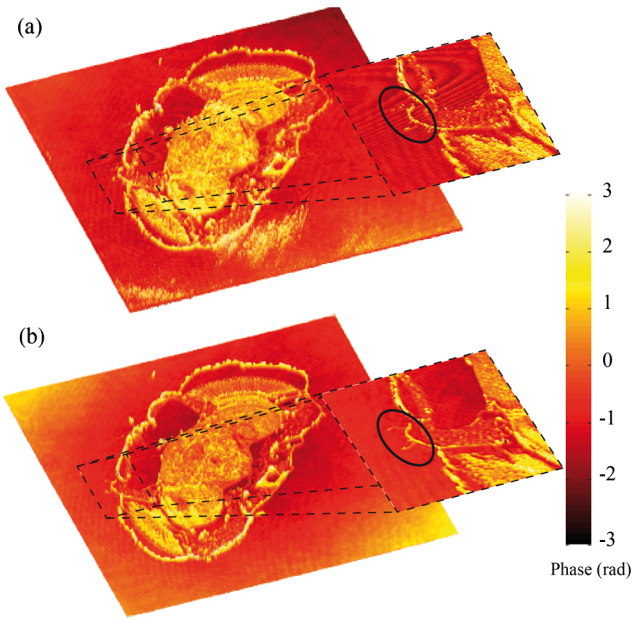

Fig. 5 (a) 3-D pseudocolor image of the phase map shown in Fig. 3(c). (b) 3-D pseudocolor image of the phase map shown in Fig. 3(e). In both cases, the image area is 0.942×0.942 mm^2. The insets show that fine details are not visible in a nontelecentric DHM. See the horn-like structure in the ellipse-bounded area.

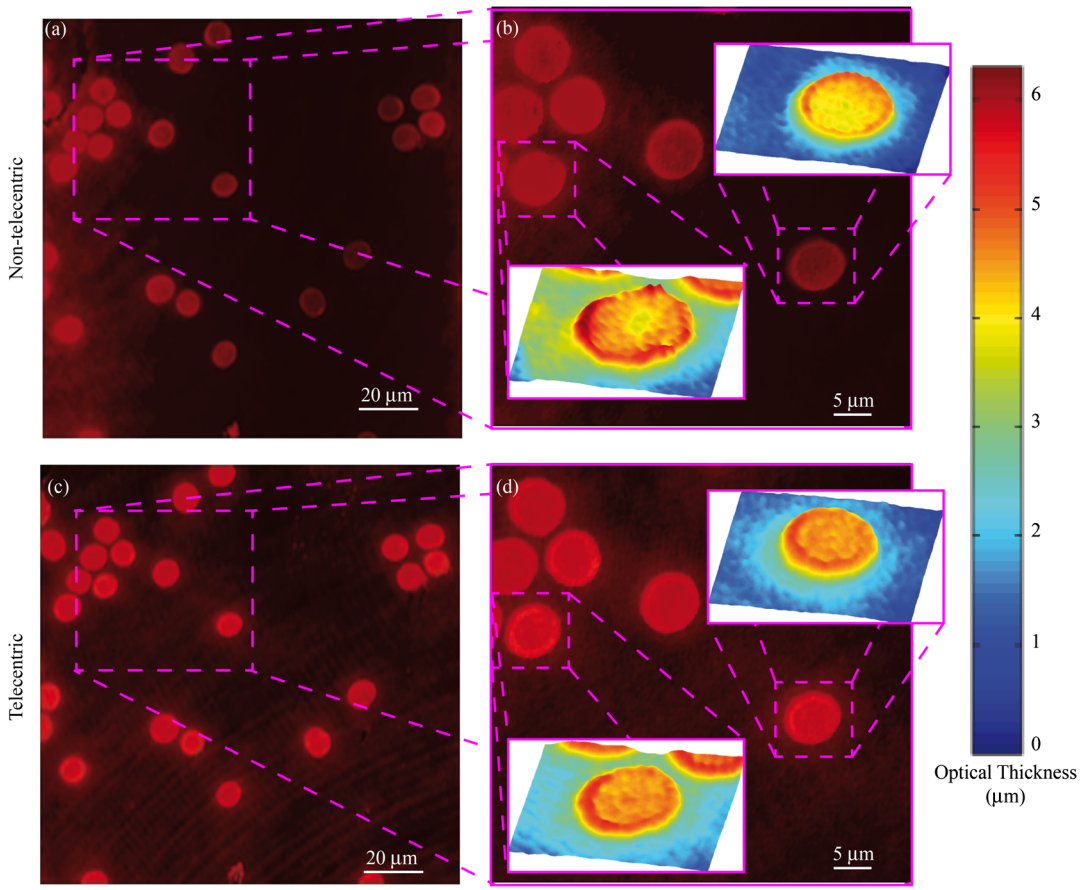

Fig. 6 Images of RBCs obtained using both nontelecentric and telecentric configurations. The inset shows that the nontelecentric imaging system introduces distortions on the measured physical thickness.

or others diagnostics that resort on label-free imaging of transparent or semitransparent samples.

4 Conclusion

The utilization of a telecentric imaging system to record the digital holograms in DHM shows noticeable advantages in the overall performance of the microscope for label-free imaging. The most remarkable benefit is that no curvature phase distortions are introduced in the recorded holograms. Therefore, the regularly required numerical compensation approaches are no longer needed. This feature circumvents, among others, the following drawbacks:

- Reduction of the usable FOV: For the numerical compensation of the remaining phase curvature, the recorded hologram should exhibit an area free of specimen such that a uniform phase is initially measured. The larger the free area, the more accurate is the numerical phase compensation. This condition to achieve accurate phase measurements imposes the shrinkage of the usable FOV.
- Remaining phase curvature: Even though for the case in which enough area is available for computing the numerical phase compensation, minimal errors in this process render anomalous phase measurements. The remaining phases typically raise the absolute measurements and/or distort the morphology of the studied specimen. The above conditions can be deleterious, for instance, in illness screening, specimen identification, and morphological classification.

The performance of the telecentric DHM allows the user to have an accurate single-shot label-free imaging system for studying transparent or semitransparent samples.

Acknowledgments

Financial support by the Ministerio de Economia y Competitividad, Spain (Grant DPI2012-32994) and the GeneralitatValenciana (Grant PROMETEO2009-077) is gratefully acknowledged. A. Doblas gratefully acknowledges funding from the University of Valencia through the predoctoral fellowship program Atracció de Talent. J. Garcia-Sucerquia gratefully acknowledges the financial support from University of Valencia, Spain, under the program Estancias Temporales para Investigadores Invitados, Colciencias grant number 110205024, and UNAL grants numbers 110201003 and 110201004.

References

1. B. Kemper et al., "Investigation on living pancreas tumor cells by digital holographic microscopy," *J. Biomed. Opt.* **11**(3), 034005 (2006).
2. N. Pavillon et al., "Early cell death detection with digital holographic microscopy," *PLoS ONE* **7**(1), e30912 (2012).
3. J. Kühn et al., "Label-free cytotoxicity screening assay by digital holographic microscopy," *Assay Drug Dev. Technol.* **11**(2), 101–107 (2013).

4. M. Puthia et al., "Prevention and treatment of colon cancer by peropal administration of HAMLET (human α-lactalbumin made lethal to tumour cells)," *Gut* **63**, 132–142 (2014).
5. K. Jeong, J. J. Turek, and D. D. Nolte, "Fourier-domain digital holographic optical coherence imaging of living tissue," *Appl. Opt.* **46** (22), 4999–5008 (2007).
6. J. Kuhn et al., "Submicrometer tomography of cells by multiple-wavelength digital holographic microscopy in reflection," *Opt. Lett.* **34**(5), 653–655 (2009).
7. N. Warnasooriya et al., "Imaging gold particles in living cell environments using heterodyne digital holographic microscopy," *Opt. Express* **18**(4), 3264–3273 (2010).
8. B. Kemper et al., "Label-free quantitative cell division monitoring of endothelial cells by digital holographic microscopy," *J. Biomed. Opt.* **15**(3), 036009 (2010).
9. H. Sun et al., "Visualization of fast-moving cells *in vivo* using digital video microscopy," *J. Biomed. Opt.* **13**(1), 014007 (2008).
10. C. J. Mann, L. Yu, and M. K. Kim, "Movies of cellular and sub-cellular motion by digital holographic microscopy," *Biomed. Eng. Online* **5**(21), 1–10 (2006).
11. D. Carl et al."Parameter-optimized digital holographic microscope for high-resolution living-cell analysis," *Appl. Opt.* **43**(36), 6536–6544 (2004).
12. Y. Emery et al., "MEMS and MOEMS resonant frequencies analysis by digital holography microscopy (DHM)," *Proc. SPIE* **8614**, 86140A (2013).
13. A. Asundi, *Digital Holography for MEMS and Microsystem Metrology*, Wiley, Chichester (2011).
14. G. Coppola et al., "Characterization of MEMS structures by microscopic digital holography," *Proc. SPIE* **4945**, 71 (2003).
15. N. Pavillion et al., "Cell morphology and intracellular ionic homoestasis explored with a multimodal approach combining epifluorescence and digital holographic microscopy," *J. Biophotonics* **3**(7), 432–436 (2010).
16. P. Marquet et al., "Red blood cell structure and dynamics explored with digital holographic microscopy," *Proc. SPIE* **7182**, 71821A (2009).
17. B. Rappaz et al., "Simultaneous cell morphometry and refractive index measurement with dual-wavelength digital holographic microscopy and dye-enhanced dispersion of perfusion medium," *Opt. Lett.* **33**(7), 744–746 (2008).
18. D. Boss et al., "Measurement of absolute cell volume, osmotic membrane water permeability, and refractive index of transmembrane water and solute flux by digital holographic microscopy," *J. Biomed. Opt.* **18** (3), 036007 (2013).
19. B. Rappaz et al., "Measurement of the integral refractive index and dynamic cell morphometry of living cells with digital holographic microscopy," *Opt. Express* **13**(23), 9361–9373 (2005).
20. I. Moon et al., "Automated three-dimensional identification and tracking of micro/nanobiological organisms by computational holographic microscopy," *Proc. IEEE* **97**(6), 990–1010 (2009).
21. A. Mölder et al., "Non-invasive, label-free cell counting and quantitative analysis of adherent cells using digital holography," *J. Microsc.* **232**(2), 240–247 (2008).
22. B. Rappaz et al., "Noninvasive characterization of the fission yeast cell cycle by monitoring dry mass with digital holographic microscopy," *J. Biomed. Opt.* **14**(3), 034049 (2009).
23. I. Moon and B. Javidi, "Three-dimensional identification of stem cells by computational holographic imaging," *J. R. Soc. Interface* **4**(13), 305–313 (2007).
24. D. Shin et al., "Optofluidic system for three-dimensional sensing and identification of micro-organisms with digital holographic microscopy," *Opt. Lett.* **35**(23), 4066–4068 (2010).
25. Z. Wong et al., "Spatial light interference microscopy (SLIM)," *Opt. Express* **19**(2), 1016–1026 (2011).
26. Z. Wong et al., "Spatial light interference tomography (SLIT)," *Opt. Express* **19**(21), 19907–19919 (2011).
27. M. K. Kim, "Principles and techniques of digital holographic microscopy," *SPIE Rev.* **1**, 018005 (2010).
28. P. Picart and J.-C. Li, *Digital Holography*, Wiley, Chichester (2012).
29. T. Kreis, *Handbook of Holographic Interferometry: Optical and Digital Methods*, Wiley, Chichester (2004).
30. G. Popescu, *Quantitative Phase Imaging of Cells and Tissues*, McGraw-Hill, New York (2011).
31. A. Doblas et al., "Shift-variant digital holographic microscopy: inaccuracies in quantitative phase imaging," *Opt. Lett.* **38**(8), 1352–1354 (2013).
32. E. Sánchez-Ortiga et al., "Digital holographic microscopy with pure-optical spherical phase compensation," *J. Opt. Soc. Am. A* **28**(7), 1410–1417 (2011).
33. T. Colomb et al., "Numerical parametric lens for shifting, magnification, and complete aberration compensation in digital holography microscopy," *J. Opt. Soc. Am. A* **23**(12), 3177–3190 (2006).
34. T. Colomb et al., "Total aberrations compensation in digital holographic microscopy with a reference conjugated hologram," *Opt. Express* **14** (10), 4300–4306 (2006).
35. J. Di et al., "Phase aberration compensation of digital holographic microscopy based on least square surface fitting," *Opt. Commun.* **282**(19), 3873–3877 (2009).
36. K. W. Seo et al., "Aberration compensation for objective phase curvature in phase holographic microscopy," *Opt. Lett.* **37**(23), 4976–4978 (2012).
37. D. P. Kelly et al., "Resolution limits in practical digital holographic systems," *Opt. Eng.* **48**(9), 095801 (2009).
38. C. Mann et al., "High-resolution quantitative phase-contrast microscopy by digital holography," *Opt. Express* **13**(22), 8693–8698 (2005).
39. P. Ferraro et al., "Compensation of the inherent wave front curvature in digital holographic coherent microscopy for quantitative phase-contrast imaging," *Appl. Opt.* **42**(11), 1938–1946 (2003).
40. B. Bhaduri et al., "Diffraction phase microscopy with white light," *Biomed. Opt. Express* **4**(8), 1434–1441 (2013).
41. B. Bhaduri, K. Tangella, and G. Popescu, "Fourier phase microscopy with white light," *Opt. Lett.* **37**(6), 1094–1096 (2012).
42. J. W. Goodman, *Introduction to Fourier Optics*, McGraw-Hill, New York (1996).
43. D. P. Kelly et al., "Quantifying the 2.5D imaging performance of digital holographic systems," *J. Eur. Opt. Soc.* **6**, 11034 (2011).
44. E. Cuche, P. Marquet, and C. Depeursinge, "Spatial filtering zero-order and twin-image elimination in digital off-axis holograhpy," *Appl. Opt.* **39**(23), 4070–4075 (2000).
45. D. Mendlovic, Z. Zalevsky, and N. Konforti, "Computation considerations and fast algorithms for calculating the diffraction integral," *J. Mod. Opt.* **44**(2), 407–414 (1997).
46. E. Cuche, P. Marquet, and C. Depeursinge, "Simultaneous amplitude-contrast and quantitative phase-contrast microscopy by numerical reconstruction of Fresnel off-axis holograms," *Appl. Opt.* **38**(34), 6994–7001 (1999).
47. J. He et al., "Light scattering by multiple red blood cells," *J. Opt. Soc. Am. A* **21**(10), 1953–1961 (2004).

Ana Doblas received her BSc and MSc degrees in physics from the University of Valencia, Spain, in 2010 and 2011, respectively. Since 2009, she has been working with the 3-D Imaging and Display Laboratory, University of Valencia, where she is currently running her PhD project and holds a predoctoral fellowship. Her research interests include three-dimensional (3-D) optical microscopy and image formation theory.

Emilio Sánchez-Ortiga received his MSc degree in photonics and his PhD in physics from the University of Valencia, Spain, in 2009 and 2014, respectively. From 2007 to 2013, he worked with the 3-D Imaging and Display Laboratory, University of Valencia. His research topics are related with 3-D optical microscopy and 3-D image formation theory. Currently, he is running a postdoc contract at the Faculty of Biological Sciences, University of Leeds.

Manuel Martínez-Corral received his PhD in physics from Valencia University in 1993. He is a full professor of optics at Valencia University, where he is co-leader of the 3D Imaging and Display Laboratory. Since 2010, he is fellow of SPIE. His research interests include 3D microscopy and 3D imaging and display technologies. He has published over 75 articles and given over 25 invited presentations. He is topical editor of the IEEE/OSA *Journal of Display Technology*.

Genaro Saavedra received his BSc and PhD degrees in physics from University of Valencia, Spain, in 1990 and 1996, respectively. He is currently a full professor with this university, and co-leads the 3-D Imaging and Display Laboratory. His current research interests are optical diffraction, integral imaging, 3-D high-resolution optical microscopy, and phase-space representation of scalar optical fields. He has published about 50 technical articles on these topics in major journals and three chapters in scientific books. He has published over 50 conference proceedings, including 10 invited presentations.

Jorge Garcia-Sucerquia received his PhD in physics from the Universidad de Antioquia at Medellin-Colombia in 2003. From 2004 to 2006, he held a postdoctoral position at Dalhousie University, Halifax, Canada, in working on digital lensless holographic microscopy. From 2012 to 2013, he was a visiting professor at the Universidad de Valencia, Valencia-España. Currently, he is an associate professor at School of Physics, Universidad Nacional de Colombia, Medellin-Colombia. His main research interest is digital holographic microscopy and applications.